Observation of spin-orbit coupled polariton vortices at room temperature

Xiaokun Zhai,[1] Xiaoran Wei,[2] Peilin Wang,[3] Xuekai Ma,[4] Ying Gao,[1] Chunzi Xing,[1] Xinmiao Yang,[1] Xiao Wang,[5] Anlian Pan,[5] Marc Assmann,[6] Yu Li,[7] Yong Zhang,[3] Stefan Schumacher,[4,8,9] and Tingge Gao[1]

[1] *Department of Physics, School of Science, Tianjin University, Tianjin 300072, China*
[2] *Institute for Electric Light Sources, College of Intelligent Robotics and Advanced Manufacturing, Fudan University, Shanghai 200433, China*
[3] *Center for Applied Mathematics and KL-AAGDM, Tianjin University, Tianjin 300072, China*
[4] *Department of Physics and Center for Optoelectronics and Photonics Paderborn (CeOPP), Universität Paderborn, Warburger Strasse 100, 33098 Paderborn, Germany*
[5] *College of Materials Science and Engineering, Hunan University, Changsha 410082, China*
[6] *Department of Physics, Otto-Hahn-Str. 4a, TU Dortmund University, 44227 Dortmund, Germany*
[7] *Coordinated Innovation Center for Computable Modeling in Management Science, Tianjin University of Finance and Economics, Tianjin 300222, China*
[8] *Institute for Photonic Quantum Systems (PhoQS), Paderborn University, 33098 Paderborn, Germany*
[9] *Wyant College of Optical Sciences, University of Arizona, Tucson, AZ 85721, USA*

ABSTRACT: Spin-orbit coupling gives rise to intriguing physical phenomena in bosonic condensates, such as formation of stripe phases and domains with vortex arrays. However, how the non-Hermiticity affects the spatial distribution of spin-orbit coupled topological defects such as vortex pair is still challenging to study. In the present work, we realize a non-equilibrium room-temperature exciton polariton condensate within a microdisk potential in a liquid crystal (LC) microcavity. We use the interplay of TE-TM mode splitting and Rashba-Dresselhaus spin-orbit coupling (RDSOC) to realize electrically tunable polariton vortex pairs with locked spin and orbital angular momentum. Importantly, the non-Hermiticity of RDSOC bands leads to unidirectional transportation of the vortex pair, such that they move to the opposite edges of the microdisk depending on their spin. Our result is robust against sample imperfections and pave the way to investigate complex states of light for non-Hermitian quantum optical information processing within optoelectronic chips.

KEYWORDS: non-Hermiticity, TE-TM splitting, Rashba-Dresselhaus, spin-orbit coupling, polariton, vortex

Coupling of spin and orbital degrees of freedom of particles determines the intrinsic properties of many materials. Enabling the control of spin degrees of freedom in solids [1, 2], spin-orbit coupling (SOC) plays a critical role in spintronics and topological insulators [3–7]. In the regime of equal Rashba [8] and Dresselhaus [9] spin-orbit coupling infinite spin lifetime [10], spin helices and spin precession were demonstrated [3, 4] in a two dimensional electron gas. In bosonic cold atom condensates, synthetic spin-orbit coupling is explored, which can be controlled by careful engineering of the spin states of atoms with laser beams. There, for example the transition from a spin-mixed phase to a spin-separated phase [11] and the measurement of a stripe phase [12] in a one dimensional Rashba and Dresselhaus coupled cold atom gas have been realized. By tuning the Raman coupling strength and introducing spatially dependent detuning which creates an effective magnetic field in the RDSOC regime [13–16], vortices or vortex lattices can be formed [17–19]. In these systems, complicated arrangement of multiple lasers is needed to realize the underlying Hamiltonian with effective SOC.

In this work we demonstrate the unidirectional transportation [20, 21] for an exciton polariton vortex pair with locked spin and orbital degrees of freedom that form as robust topological defect in the Rashba-Dresselhaus regime of a photonic planar microcavity at room temperature. In such optical systems vortices formed with well defined and locked spin and orbital degrees of freedom play an increasingly important role for communication technologies and qubit manipulation schemes [22–24]. As depicted in Figure 1(a), our realization constitutes a LC planar photonic microcavity. The microcavity allows to tune the orientation of the LC molecule and related effective refractive indices with an externally applied electric field, such that an effective RDSOC [25–27] is realized with a Hamiltonian of the form $H = \hbar^2 k^2/2m + 2\alpha k_y \sigma_z$. α represents the RDSOC strength that leads to the separation of the two opposite spin components in the momentum space and real space [28](σ_z is the third component of the Pauli matrix). However, spatial separating high order polariton modes under RDSOC regime is still illusive, which are affected by the disorder or polariton-polariton interactions.

The particles underlying our system are hybrid quasiparticles, so-called exciton polaritons, that are created due to the strong coupling of excitons and cavity photons [29, 30]. Perovskites have attracted significant attention to study exciton polaritons due to the large exciton binding energy and oscillator strength and show condensation at room temperature [31–39]. Higher-order modes, such as vortices and petal-shaped patterns, can emerge spon-

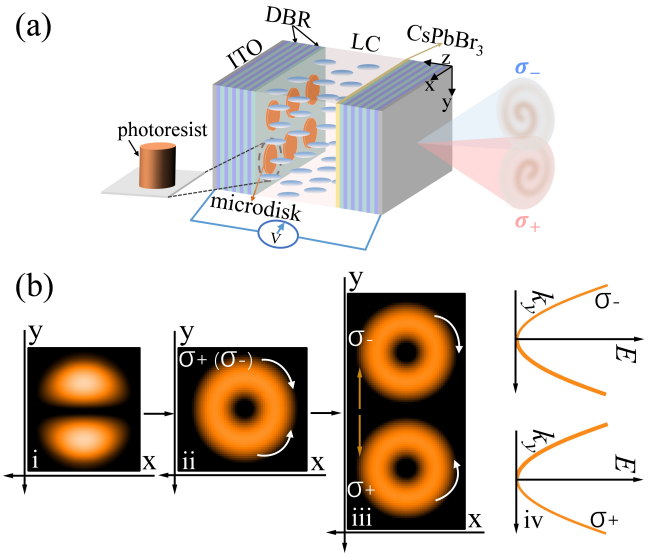

FIG. 1. **Schematic of the LC microcavity and formation of spin-orbit coupled vortex pairs.** (a) The microcavity is filled with LC and contains a microdisk array and $CsPbBr_3$ microplates facing each other. (b) Sketch of the idealized modes in the microcavity: the TE-TM splitting splits a polariton dipole mode into two spin-orbit-locked vortices spatially separated by the non-Hermitian induced unidirectional transportation in the RDSOC bands.

taneously in exciton-polariton condensates [40–47]. Especially a spin-orbit coupled polariton vortex pair can appear under TE-TM splitting, which occurs between longitudinal and transverse optical modes [48–51]. As shown in Figure 1(b), TE-TM splitting can split a dipole mode (i) into two vortices with topological charges locked with the vectorial polarization degree of freedom ((ii) in Figure 1(b)), or in other words, locked with the SAM [52, 53]. In these vortex pairs where spin and orbital degrees of freedom are locked, the vortex that is observed in one circularly polarized component (e.g., $\sigma-$) rotates in the opposite direction (e.g., clockwise) from the vortex observed in the other circularly polarized component ($\sigma+$; counter-clockwise rotation). However, these kinds of well defined spin-orbit locked modes have not been observed yet at room temperature. With only weak TE-TM splitting, a very high-quality microcavity would be required as otherwise detrimental factors such as sample disorder or interaction between polaritons tend to destroy the locking between SAM and OAM.

The polarization dependent loss [54] of the horizontal and vertical linearly polarized polariton modes can lead to asymmetric linewidth when they are brought into resonance to form non-Hermitian RDSOC bands, which indicates unidirectional transport and leads to the spin dependent spatial separation ((iii) and (iv) in Figure 1(b)) [55–57]. To elucidate the underlying mechanism, we consider the linearized dynamics of a driven–dissipative two-component polariton fluid. Assuming normal-mode solutions $\psi_\pm(\mathbf{r},t) = \phi_\pm(\mathbf{r})e^{-\mathrm{i}\,\lambda t}$ and introducing the spinor field $\Phi = (\phi_+, \phi_-)^T$, the weak-density dynamics reduces to the non-Hermitian eigenvalue problem:

$$\mathcal{F}^{-1}\big[H(\mathbf{k})\widetilde{\Phi}(\mathbf{k})\big] + V(\mathbf{r})\Phi(\mathbf{r}) = \lambda\,\Phi(\mathbf{r}), \qquad (1)$$

$$H(\mathbf{k}) = \begin{pmatrix} \frac{\hbar^2k^2}{2m} + 2\alpha k_y + \mathrm{i}\,\gamma_+(\mathbf{k}) & \beta(k_x + \mathrm{i}\,k_y)^2 \\ \beta(k_x - \mathrm{i}\,k_y)^2 & \frac{\hbar^2k^2}{2m} - 2\alpha k_y + \mathrm{i}\,\gamma_-(\mathbf{k}) \end{pmatrix}, \qquad (2)$$

where $\widetilde{\Phi} = \mathcal{F}[\Phi]$ and $k^2 = k_x^2 + k_y^2$. $\mathcal{F}(\Phi)$ is the Fourier transform of function Φ. The momentum-space Hamiltonian encodes kinetic dispersion, the linear spin–orbit shifts $\pm 2\alpha k_y$, TE–TM mixing $\beta(k_x \pm \mathrm{i}\,k_y)^2$, and the momentum-dependent non-Hermitian linewidths $\gamma_\pm(\mathbf{k})$, while the real-space potential $V(\mathbf{r})$ stabilizes ring-shaped vortex modes. In the Hermitian limit $\gamma_\pm(\mathbf{k}) = 0$, Eq. (1) yields the reference vortex modes shown in Figure 2(a–d). Both spin components form perfectly concentric ring-shaped densities and carry opposite 2π phase windings, resulting in a single vortex core centered exactly at the origin for both $\sigma+$ and $\sigma-$ components. These modes provide the baseline against which dissipative symmetry breaking can be unambiguously identified.

To induce dissipative symmetry breaking, we allow the linewidths $\gamma_\pm(\mathbf{k})$ to acquire a weak momentum dependence such that their minima are displaced in opposite directions along k_y on the spin–orbit scale $\Delta = 2m\alpha$ (the model parameters are listed in the SM.). This construction explicitly breaks the reflection symmetry $k_y \to -k_y$ while leaving the Hermitian part of the spectrum unchanged. In the resulting non-Hermitian problem stationary modes are no longer selected by energy alone but by minimizing their net decay rate. Consequently, the $\sigma+$ component redistributes its spectral weight toward positive k_y, where γ_+ is smallest, whereas the $\sigma-$ component shifts toward negative k_y, where γ_- is minimized. These opposite momentum-space redistributions translate directly into real space as displaced vortex cores, as shown in Figure 2(e–h): the $\sigma+$ vortex shifts downward, while the $\sigma-$ vortex shifts upward. The relative displacement of the two cores thus provides a clear and direct signature of dissipative symmetry breaking. Importantly, the separation distances of the two vortex cores are not identical. Although the momentum-dependent dissipation shifts the spectral weight of the $\sigma+$ and $\sigma-$ components toward opposite halves of momentum space, the resulting real-space displacements need not be equal in magnitude. Due to the spin–orbit–induced momentum offset, the two spin components experience different effective angular coordinates in momentum space, leading to unequal angular-momentum mixing under the Fourier–Bessel transformation. Consequently, the amplitudes of the induced real-space shifts differ for $\sigma+$ and $\sigma-$, result-

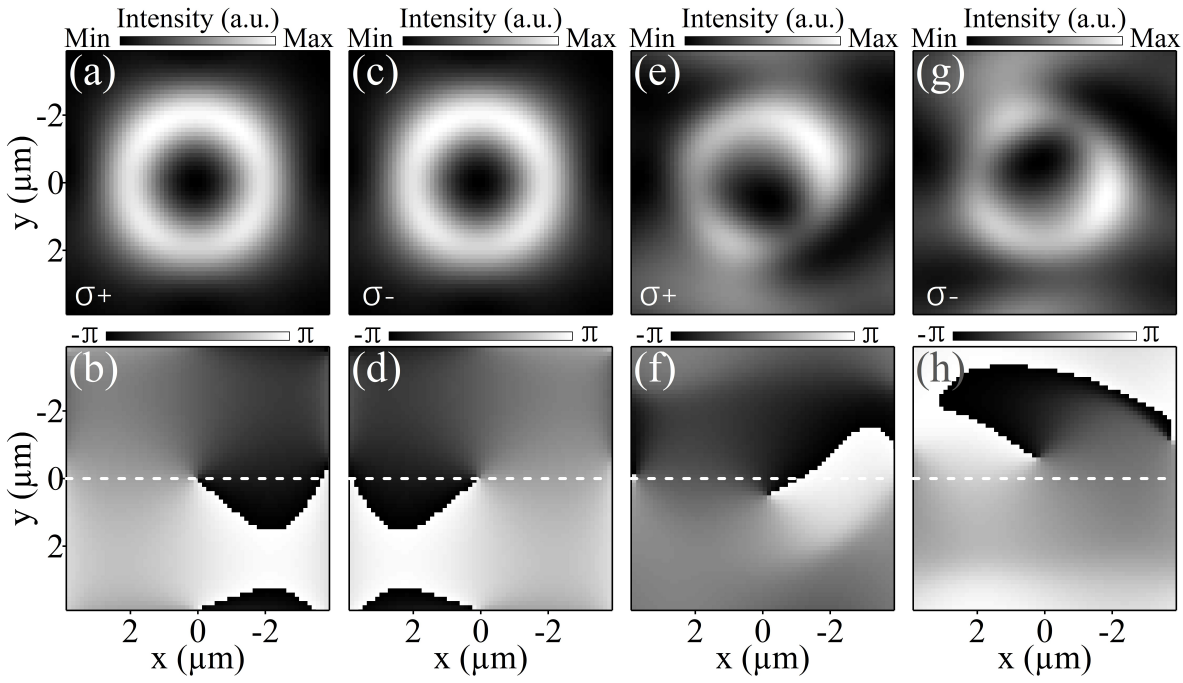

FIG. 2. **Theoretical simulation of the spin-orbit coupled vortex pairs.** (a, c) Real-space images of exciton-polariton distributions for $\gamma_{\pm}(\mathbf{k}) = 0$. (b, d) Corresponding phase distributions for (a) and (c), respectively. (e, g) Real-space images for $\gamma_{\pm}(\mathbf{k}) \neq 0$. (f, h) Corresponding phase distributions for (e) and (g), respectively. The dashed lines in (b, d) and (f, h) indicate the zero-position reference.

ing in asymmetric vortex-core separations. A detailed analytical derivation of this effect is provided in the SM.

Based on the theoretical simulation, we experimentally show two spin-orbit coupled vortices created under TE-TM splitting are spatially separated through the non-Hermiticity induced unidirectional transport of the RDSOC bands, such that each spin component of the polariton condensate carries a distinct OAM and moves towards the opposite edge of the potential trap. The formation of spin-orbit locked vortex pairs can be directly observed by measuring the left- and right-circularly polarized emission at room temperature. These findings are robust against disorder within the microcavity. Our results demonstrate a different mechanism to electrically create and separate vortex pairs with locked spin and orbital degrees of freedom via the non-Hermitian in a photonic quantum fluid, offering a platform to investigate non-Hermitian topology in spin-orbit-coupled bosonic condensates.

In the experiment we introduce photoresist microdisk structures with the diameter of 4 μm (the distance between the microdisk is around 15 μm to avoid interaction, as detailed in the SM) and the height of 120 nm onto the bottom Distributed Bragg Reflector (DBR) using lithography technique in the LC microcavity, where the effective cavity length of the microdisk is larger and the cavity mode energy is smaller compared with other area. In this case, the microdisks act as potential traps and polaritons are confined in these structures, occupying the specific discrete energy levels [58, 59], for example, a dipole mode. The size of the inserted $CsPbBr_3$ microplates is around 40 μm which can cover at least one microdisk potential. We use a linearly polarized laser (repetition rate: 1 kHz, wavelength: 400 nm, pulse width: 50 fs) to excite the microcavity with the size of around 50 μm.

We measure the dispersion of the LC microcavity as the same as [31] below threshold when the voltage is 5 V, which is plotted in Figure 3(a). Multiple polariton branches are observed when the pumping density is far below the threshold due to the large thickness of the cavity. That is, several cavity modes exist within the microcavity and strongly couple with the excitons (detailed fitting parameters are shown in the SM). The strong coupling is confirmed at the large-wavevector region where one can clearly observe that the dispersions become flat when approaching the exciton resonance. Under this voltage, the LP1 and LP3 are horizontally linearly polarized whereas the LP2 and LP4 are vertically linearly polarized.

With further increasing the pumping density to around 18 $\mu J/cm^2$, the emitted PL intensity of the polaritons increases superlinearly, whereas the linewidth drops suddenly and the polariton energy shows noticeable continuous blueshift (details in SM). These results clearly show the occurrence of the polariton condensation at the lower branch LP2 (Figure 3(b)). We note that the thresholds of

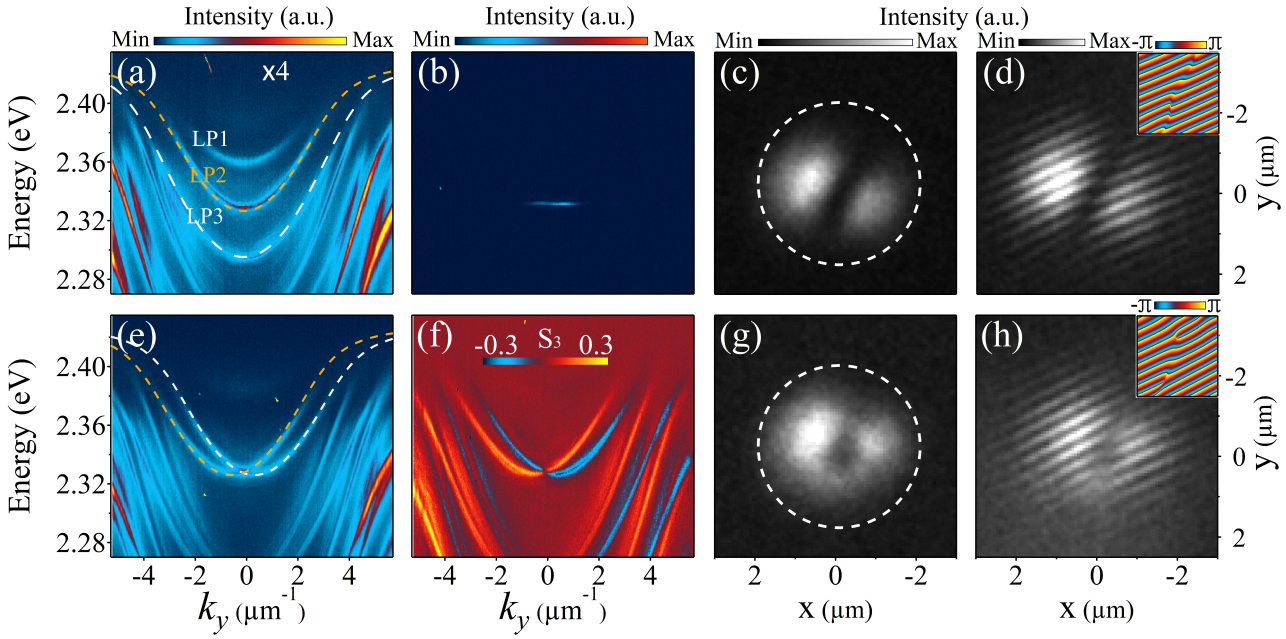

FIG. 3. **Polariton condensation in the LC microcavity at different voltages.** (a, b) Dispersion below and above threshold at 5 V. (c, d) Real space image and interferogram of the polariton condensate at 5 V. (e) Dispersion below threshold at 5.6 V. (f) Spin polarized (S_3 component) dispersion at 5.6 V, defined as $(I_{\text{left}}\text{-}I_{\text{right}})/(I_{\text{left}}+I_{\text{right}})$ where I_{left} (I_{right}) is the left(right)-hand circularly polarized dispersion. Fitted curves are the simulated bands using a coupled oscillator model (a) and a four-band Hamiltonian [28] (e). (g, h) Real space image and interferogram of the polariton condensate at 5.6 V. The dashed lines in (c, g) indicate the microdisk. The insets in (d, h) show the extracted phase.

the modes in the microdisk potential can vary in a certain range, depending on the external pumping, relaxation and decay of polaritons [60–62]. By carefully selecting the microdisk size, thickness, and pumping conditions, we ensure that the polariton condensate forms a single dipole mode in real space above threshold, as shown in Figure 3(c). We set the pumping density to be around 1.2 P_{th} where the nonlinearity can be neglected. We build a Michelson interferometer where one arm is expanded by around 15 times and acts as the reference beam. Clear interference fringes are observed above the threshold (Figure 3(d)), the extracted phase from the Fast Fourier transformation of the fringes shown in the upper right corner indicates the development of the macroscopic coherence across the condensate and the phase jump of π across the two lobes.

The TE-TM splitting is prominent in anisotropic perovskite or LC-based microcavities [63–65], which can decompose the above dipole mode into two vortices with the topological charge of ± 1, locked with the SAM. However, it is noteworthy that the disorder in the perovskite microplates or the fabricated photoresist microdisk can perturb the coherent formation of vortices. Furthermore, polariton-polariton interactions may also degrade the locking between the SAM and OAM , thereby preventing the clear observation of spin-orbit locked vortex states. As analyzed above, these two vortices can be directly measured in the non-Hermitian RDSOC regime, which can be realized by simply increasing the voltage in our experiments. When the voltage is increased to 5.6 V, the polariton branch LP3 is blueshifted to be resonant with LP2. These two polariton branches have the opposite linear polarizations and parity, thus the RD spin split bands form (please see the total (Figure 3(e)) and spin polarized (Figure 3(f)) dispersion). Under the same pumping density of Figure 3(c), polaritons condense and the dipole mode becomes deformed under the same pumping density (shown in Figure 3(g)) where the polariton condensate carries a ring shape, indicating the formation of vortices. The interferogram of the polariton condensate in Figure 3(h) shows the emergence of two forks oriented in opposite directions. This confirms the existence of two vortices with the topological charge of ± 1 close to the core region of the ring-shaped condensate, which can be unambiguously proven by the extracted phase plotted at the upper right corner, calculated by using the same method as in Figure 3(d).

To check whether the two vortices are locked with the definite SAM as we analyzed above, we measure the right- and left-hand circularly polarized PL emitted from the microcavity, which correspond to different spins states of the polariton condensate. In Figure 4(a), an intensity minimum in the center of the polariton condensate is clearly visible in the $\sigma+$ component, indicating the exis-

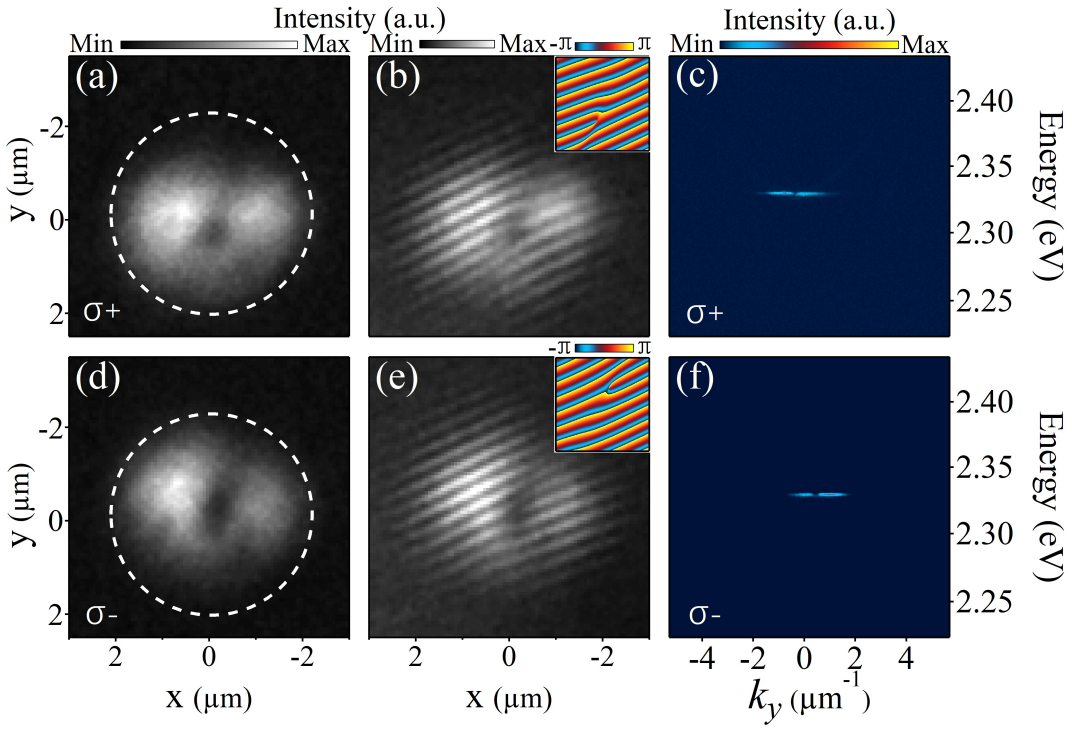

FIG. 4. **Spin-orbit locked polariton vortex pair at 5.6 V.** (a, b, c) Real space image, interferogram and dispersion of the $\sigma+$ component at 5.6 V. (d, e, f) Real space image, interferogram and dispersion of the $\sigma-$ component at 5.6 V. The dashed lines in (a) and (d) indicate the microdisk. The insets in (b) and (e) are the extracted phase indicating the vortex.

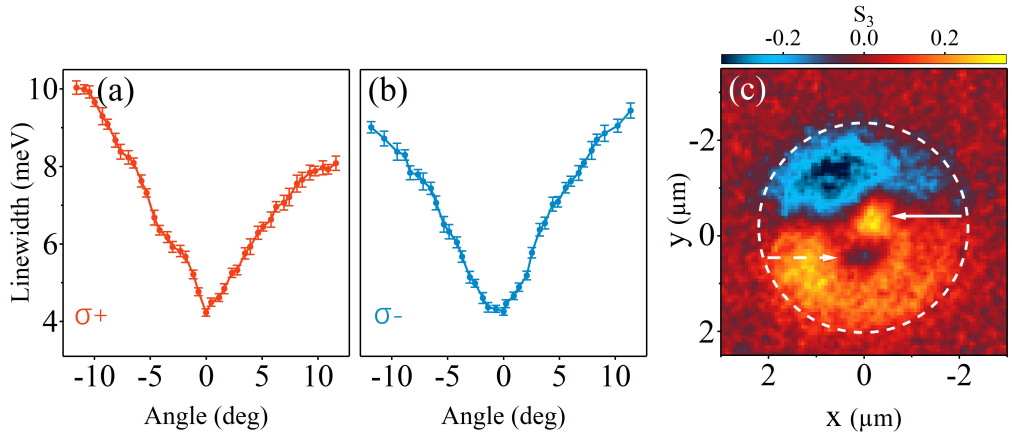

FIG. 5. **Unidirectionnal transportation of polariton vortex pair in the RDSOC bands.** (a) Linewidth of the polariton modes in the $\sigma+$ component at 5.6 V. (b) Linewidth of the polariton modes in the $\sigma-$ component at 5.6 V. Horizontal axis of (a) and (b) is shifted respectively to make the ground state of the two spin components to be at 0 for the clarity of the linewidth analysis. (c) Spin polarized real space images of the vortex pair. The arrows indicate the location of the two vortex cores. The dashed lines in (c) indicate the microdisk.

tence of a vortex. We note that the intensity distribution is not very symmetric around the intensity minimum, this is due to the inhomogeneity within the microcavity. From the interferogram by superimposing the real space image of the polariton condensate onto the reference arm, a fork is clearly observed, confirming the appearance of a vortex with the topological charge of -1, as plotted in Figure 4(b). The phase singularity can also be seen in the calculated phase distribution inserted at the upper right corner. From the dispersion taken under this voltage (Figure 4(c)), two peaks are observed to be located at the wavevector of 0.12 μm^{-1} and -0.88 μm^{-1}, which is not symmetric along the normal incidence due to the RDSOC induced shift along k_y direction. This kind of

particular distribution of the dispersion confirms the appearance of the vortex with asymmetric distribution in the momentum space and a downward spatial shift in real space for the $\sigma+$ component.

On the other hand, for the $\sigma-$ component, both the intensity minimum in the real space image (Figure 4(d)) and the fork in the interferogram graph (Figure 4(e)) demonstrate the formation of the vortex with the topological charge of +1. Moreover, the location of the polariton condensate is shifted upwards within the microdisk confinement potential. In this spin component, the polariton condensate distribution in the momentum space is also shifted to the opposite direction compared to Figure 4(c), with the peak locations at 0.98 μm^{-1} and -0.07 μm^{-1} (Figure 4(f)). The mode distribution of the dispersion clearly confirms the existence of the swapped topological charge of the vortex in the $\sigma-$ component.

The appearance of the spin-orbit locked polariton vortex pair under 5.6 V originates from the synthetic magnetic field due to the RDSOC and the prominent TE-TM splitting. The nonzero TE-TM splitting can be confirmed by measuring the two linearly polarized dispersions along k_x direction when $k_y = 0$ (where the RDSOC disappears), which reveal two parabolic dispersions with a distinct energy splitting corresponding to the TE and TM polarized modes, respectively, as detailed in the SM. In our experiments, the TE-TM splitting decomposes the dipole mode into two spin-orbit locked vortices, whereas the spatial distribution of the two vortices is deeply affected by the non-Hermiticity of RDSOC bands. Experimentally, we calculate the linewidth of the polariton bands of the $\sigma+$ component below threshold based on the data in Figure 3(e) in the RDSOC regime, which show a clear asymmetric distribution along k_y and -k_y direction (Figure 5(a)). The linewidth of the polaritons along k_y direction is smaller than -k_y direction when their energy is the same, this means the vortex with the topological charge of -1 will propagate unidirectionally along $+y$ direction and accumulate at the bottom edge of the microdisk. For $\sigma-$ component, vortex with the topological charge of +1 will show opposite transportation behavior due to opposite asymmetry of the linewidth distribution (Figure 5(b)). This clearly indicates the unidirectional transportation in the spin-orbit coupled polariton vortex pair within the RDSOC bands. Thanks to the spatially separation of the two vortices towards the edge of the microdisk, the inter-species interaction can be reduced. In this case, the two vortices can be observed directly by measuring polarization resolved PL in the experiment. The spin polarized real space image of the polariton condensate at 5.6 V plotted in Figure 5(c) demonstrates the separation of the two vortices along $\pm y$ direction with two cores clearly visible indicated by the arrows. The spatial separation of the spin-orbit coupled vortex pair can be reproduced in other area within the same microcavity, as shown in the SM, this shows that our results are robust against possible disorders within the microcavity.

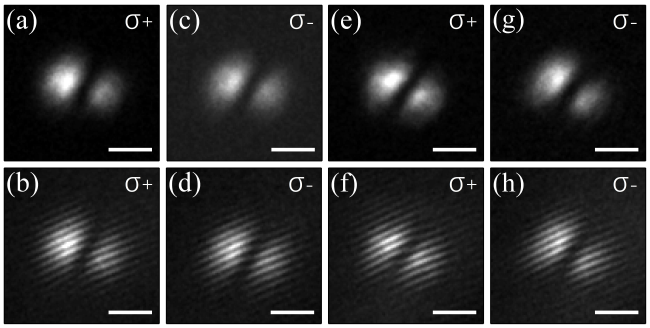

FIG. 6. **Polarization dependence of polariton condensates outside the RDSOC regime.** (a, b) Real space image and interferogram of the $\sigma+$ polarized component of the polaritons at 5 V. (c, d) Real space image and interferogram of the $\sigma-$ polarized component of the polaritons at 5 V. (e-h) Same as (a-d) but for an external voltage of 6 V. The scale bars: 2 μm.

If the RDSOC spin splitting disappears, for example, at 5 V where the polariton mode LP3 is far below LP2, the spin-orbit coupling vanishes. As a result, the two spin components of the polariton condensate share the same spatial mode distribution in the real space without definite vorticity and spin polarization (Figure 6(a-d)). When the voltage applied to the microcavity is increased to 6 V (such that LP3 is tuned above LP2; see the SM), the polariton condensate also assumes a dipole shape. The $\sigma+$ and $\sigma-$ spin-polarized components of the polariton condensate again show the same spatial mode without vorticity due to the absence of the SOC (Figure 6(e-h)). This confirms that the TE-TM splitting alone is insufficient to stabilize the observed vortex pair in our microcavity. When the system is tuned away from the RD regime (e.g., at 5 V or 6 V), the nonlinear interaction and possible disorder make the vortex unstable, thus we observe the dipole modes.

Compared with other optically tunable spin-orbit coupled photonic vortex lasers [23, 24, 66] or polariton vortices confined in micropillar structures, which so far are limited to cryogenic temperature [60], our work shows the RDSOC bands can separate unidirectionally the spin-orbit coupled vortex pair in the real space, and lays the foundation to manipulate electrically tunable state with spin-orbit coupled angular momentum at room temperature.

To summarize, we observe the unidirectional transporation for a spin-orbit locked polariton vortex pair in a LC microcavity. The spin-orbit locked polariton vortices originate from the TE-TM splitting. They become observable due to the separation of the condensate resulting from the non-Hermiticity induced unidirectional transportation behavior within the RDSOC bands for different spin component. Our results illustrate an important

electrical method for the manipulation of the spin-orbit locked topological defects based on a quantum fluid of light at room temperature, and pave the way to investigate vortex pair underlying quantum statistics [67] using macroscopically coherent states of hybrid light-matter particles at room temperature. These observations are of interest also for other areas such as cold atom gases and 2D electron gases in which the targeted design of non-Hermitian spin-orbit locked states is often not accessible or much more complex to achieve.

SUPPORTING INFORMATION

Theoretical parameters for spin-orbit coupled vortex pairs, fabrication details and structural characterization of photoresist microdisk structures, supplementary experimental data and analysis of room-temperature polariton condensation, quantitative measurement and verification of TE-TM splitting, the asymmetry of the linewidth above threshold,experimental demonstration of spin-orbit coupled vortex pairs in other regions of the same microcavity, dispersion curves at 6 V.

AUTHOR INFORMATION

Corresponding Author Email: xiaokunzhai@tju.edu.cn; tinggegao@tju.edu.cn

ACKNOWLEDGMENTS

T.G. acknowledges support from the National Natural Science Foundation of China (grant No. 12174285). The Paderborn group acknowledges support by the Deutsche Forschungsgemeinschaft (German Research Foundation) through the transregional collaborative research center TRR142/3-2022 (231447078, project A04) and by Paderborn Center for Parallel Computing, PC^2. X.Z. acknowledges support from the National Natural Science Foundation of China(NSFC, No. 12504372) and the China Postdoctoral Science Foundation - Tianjin Joint Support Program under Grant Number (No. 2025T003TJ). Y.Z. acknowledges support from the National Natural Science Foundation of China (Grant No. 12271400), the National Key R&D Program of China (Grant No. 2024YFA1012803), and the Basic Research Fund of Tianjin University (Grant No. 2025XJ21-0010).

DATA AVAILABILITY STATEMENT

The data that support the findings of this study are available from the corresponding author upon reasonable request.

REFERENCES

[1] A. Manchon, H. C. Koo, J. Nitta, S. M. Frolov, R. A. Duine, New perspectives for Rashba spin–orbit coupling. *Nature Materials* **14,** 871-882 (2015).

[2] R. Winkler, S. J. Papadakis, E. P. De Poortere, M. Shayegan, *Advances in Solid State Physics: Spin-orbit coupling in two-dimensional electron and hole systems,* vol 41 (Springer, Berlin, Heidelberg. 2003).

[3] Y. K. Kato, R. C. Myers, A. C. Gossard, D. D. Awschalom, Observation of the spin Hall effect in semiconductors. *Science* **306,** 1910-1913 (2004).

[4] M. König, S. Wiedmann, C. Brüne, A. Roth, H. Buhmann, L. W. Molenkamp, X. L. Qi, S. C. Zhang, Quantum spin Hall insulator state in HgTe quantum wells. *Science* **318,** 766-770 (2007).

[5] C. L. Kane, E. J. Mele, Z_2 topological order and the quantum spin Hall effect. *Physical Review Letters* **95,** 146802 (2005).

[6] B. A. Bernevig, T. L. Hughes, S. -C. Zhang, Quantum spin Hall effect and topological phase transition in HgTe quantum wells. *Science* **314,** 1757-1761 (2006).

[7] D. Hsieh, D. Qian, L. Wray, Y. Xia, Y. S. Hor, R. J. Cava, M. Z. Hasan, A topological Dirac insulator in a quantum spin Hall phase. *Nature* **452,** 970-974 (2008).

[8] E. I. Rashba, Properties of semiconductors with an extremum loop. I. Cyclotron and combinational resonance in a magnetic field perpendicular to the plane of the loop. *Soviet physics-Solid state* **2,** 1109-1122 (1960).

[9] G. Dresselhaus, Spin-orbit coupling effects in zinc blende structures. *Physical Review* **100,** 580 (1955).

[10] B. A. Bernevig, J. Orenstein, S. C. Zhang, Exact SU(2) symmetry and persistent spin helix in a spin-orbit coupled system. *Physical Review Letters* **97**, 236601 (2006).

[11] Y. J. Lin, K. Jiménez-García, I. B. Spielman, Spin–orbit-coupled Bose–Einstein condensates. *Nature* **471,** 83-86 (2011).

[12] J. R. Li, J. Lee, W. Huang, S. Burchesky, B. Shteynas, F. C. Top, A. O. Jamison, W. Ketterle, A stripe phase with supersolid properties in spin–orbit-coupled Bose–Einstein condensates. *Nature* **543,** 91-94 (2017).

[13] Y. Li, L. P. Pitaevskii, S. Stringari, Quantum tricriticality and phase transitions in spin-orbit coupled Bose-Einstein condensates. *Physical Review Letters* **108**, 225301 (2012).

[14] G. I. Martone, Y. Li, L. P. Pitaevskii, S. Stringari, Anisotropic dynamics of a spin-orbit-coupled Bose-Einstein condensate. *Physical Review A* **86**, 063621 (2012).

[15] H. Zhai, Degenerate quantum gases with spin–orbit coupling: a review. *Reports on Progress in Physics* **78,** 026001 (2015).

[16] J. Ren, T. Long, C. Gu, H. Fu, D. Solnyshkov, G. Malpuech, Q. Liao, Optical spin Hall effect pattern switching in polariton condensates in organic single-crystal microbelts. *Journal of the American Chemical Society* **147,** 8336-8342 (2025).

[17] C. Wang, C. Gao, C. M. Jian, H. Zhai, Spin-orbit coupled spinor Bose-Einstein condensates. *Physical Review Letters* **105,** 160403 (2010).

[18] J. Radić, T. A. Sedrakyan, I. B. Spielman, V. Galitski, Vortices in spin-orbit-coupled Bose-Einstein condensates. *Physical Review A* **84,** 063604 (2011).

[19] I. B. Spielman, Raman processes and effective gauge potentiais. *Physical Review A* **79,** 063013 (2009).

[20] S. Mandal, R. Banerjee, E. A. Ostrovskaya, T. C. H. Liew, Nonreciprocal transport of exciton polaritons in a non-Hermitian chain. *Physical Review Letters* **125,** 123902 (2020).

[21] H. Xu, K. Dini, X. Xu, R. Banerjee, S. Mandal, T. C. H. Liew, Nonreciprocal exciton-polariton ring lattices. *Physical Review B* **104,** 195301 (2021).

[22] N. Bozinovic, Y. Yue, Y. Ren, M. Tur, P. Kristensen, H. Huang, A. E. Willner, S. Ramachandran, Terabit-scale orbital angular momentum mode division multiplexing in fibers. *Science* **340,** 1545-1548 (2013).

[23] Z. Zhang, H. Zhao, S. Wu, T. Wu, X. Qiao, Z. Gao, R. Agarwal, S. Longhi, N. M. Litchinitser, L. Ge, L. Feng, Spin–orbit microlaser emitting in a four-dimensional Hilbert space. *Nature* **612,** 246–251 (2022).

[24] Z. Zhang, X. Qiao, B. Midya, K. Liu, J. Sun, T. Wu, W. Liu, R. Agarwal, J. M. Jornet, S. Longhi, N. M. Litchinitser, L. Feng, Tunable topological charge vortex microlaser. *Science* **368,** 760–763 (2020).

[25] K. Rechcińska, M. Król, R. Mazur, P. Morawiak, R. Mirek, K. Łempicka, W. Bardyszewski, M. Matuszewski, P. Kula, W. Piecek, P. G. Lagoudakis, B. Piętka, J. Szczytko, Engineering spin-orbit synthetic Hamiltonians in liquid-crystal optical cavities. *Science* **366,** 727-730 (2019).

[26] M. Król, K. Rechcińska, H. Sigurdsson, P. Oliwa, R. Mazur, P. Morawiak, W. Piecek, P. Kula, P. G. Lagoudakis, M. Matuszewski, W. Bardyszewski, B. Piętka, J. Szczytko, Realizing optical persistent spin helix and Stern-Gerlach deflection in an anisotropic liquid crystal microcavity. *Physical Review Letters* **127,** 190401 (2021).

[27] J. Liang, W. Wen, F. Jin, Y. G. Rubo, T. C. H. Liew, R. Su, Polariton spin Hall effect in a Rashba–Dresselhaus regime at room temperature. *Nature Photonics* **18,** 357-362 (2024).

[28] Y. Li, X. Ma, X. Zhai, M. Gao, H. Dai, S. Schumacher, T. Gao, Manipulating polariton condensates by Rashba-Dresselhaus coupling at room temperature. *Nature Communications* **13,** 3785 (2022).

[29] J. Kasprzak, M. Richard, S. Kundermann, A. Baas, P. Jeambrun, J. M. Keeling, F. M. Marchetti, M. H. Szymańska, R. André, J. L. Staehli, V. Savona, P. B. Littlewood, B. Deveaud, S. L. Dang, Bose-Einstein condensation of exciton polaritons. *Nature* **443,** 409-414 (2006).

[30] R. Balili, V. Hartwell, D. Snoke, L. Pfeiffer, K. West, Bose-Einstein condensation of microcavity polaritons in a trap. *Science* **316,** 1007-1010 (2007).

[31] X. Zhai, X. Ma, Y. Gao, C. Xing, M. Gao, H. Dai, X. Wang, A. Pan, S. Schumacher, T. Gao, Electrically controlling vortices in a neutral exciton-polariton condensate at room temperature. *Physical Review Letters* **131,** 136901 (2023).

[32] Y. Gao, X. Ma, X. Zhai, C. Xing, M. Gao, H. Dai, H. Wu, T. Liu, Y. Ren, X. Wang, A. Pan, W. Hu, S. Schumacher, and T. Gao, Single-shot spatial instability and electric control of polariton condensates at room temperature. *Physical Review B* **108**, 205303(2023).

[33] M. S. Spencer, Y. Fu, A.P. Schlaus, D. Hwang, Y. Dai, M.D. Smith, D.R. Gamelin, X.-Y. Zhu, Spin-orbit coupled exciton-polariton condensates in lead halide perovskites. *Science Advances* **7,** eabj7667 (2021).

[34] R. Su, J. Wang, J. Zhao, J. Xing, W. Zhao, C. Diederichs, T. C. H. Liew, Q. Xiong, Room temperature long-range coherent exciton polariton condensate flow in lead halide perovskites. *Science Advances* **4,** eaau0244 (2018).

[35] J. Song, S. Ghosh, X. Deng, C. Li, Q. Shang, X. Liu, Y. Wang, X. Gao, W. Yang, X. Wang, Q. Zhao, K. Shi, P. Gao, G. Xing, Q. Xiong, Q. Zhang, Room- temperature continuous- wave pumped exciton polariton condensation in a perovskite microcavity. *Science Advances* **11,** eadr1652 (2025).

[36] K. Łempicka-Mirek, M. Król, L. De Marco, A. Coriolano, L. Polimeno, I. Viola, M. Kędziora, M. Muszyński, P. Morawiak, R. Mazur, P. Kula, W. Piecek, P. Fita, D. Sanvitto, J. Szczytko, B. Piętka, Electrical polarization switching of perovskite polariton laser. *Nanophotonics* **13,** 2659-2668 (2024).

[37] R. Su, S. Ghosh, J. Wang, S. Liu, C. Diederichs, T. C. H. Liew, Q. Xiong, Observation of exciton polariton condensation in a perovskite lattice at room temperature. *Nature Physics* **16,** 301-306 (2020).

[38] J. Feng, J. Wang, A. Fieramosca, R. Bao, J. Zhao, R. Su, Y. Peng, T. C. H. Liew, D. Sanvitto, Q. Xiong, All-optical switching based on interacting exciton polaritons in self-assembled perovskite microwires. *Science Advances* **7,** eabj6627 (2021).

[39] J. Wu, S. Ghosh, R. Su, A. Fieramosca, T. C. H. Liew, Q. Xiong, Nonlinear parametric scattering of exciton polaritons in perovskite microcavities. *Nano Letters* **21,** 3120-3126 (2021).

[40] K. G. Lagoudakis, M. Wouters, M. Richard, A. Baas, I. Carusotto, R. André, L. S. Dang, B. Deveaud-Plédran, Quantized vortices in an exciton-polariton condensate. *Nature Physics* **4,** 706-710 (2008).

[41] D. Sanvitto, F. M. Marchetti, M. H. Szymańska, G. Tosi, M. Baudisch, F. P. Laussy, D. N. Krizhanovskii, M. S. Skolnick, L. Marrucci, A. Lemaître, J. Bloch, C. Tejedor, L. Viña, Persistent currents and quantized vortices in a polariton superfluid. *Nature Physics* **6,** 527–533 (2010).

[42] I. Gnusov, S. Harrison, S. Alyatkin, K. Sitnik, J. Töpfer, H. Sigurdsson, P. Lagoudakis, Quantum vortex formation in the "rotating bucket" experiment with polariton condensates. *Science Advances* **9,** eadd1299 (2023).

[43] X. Ma, B. Berger, M. Assmann, R. Driben, T. Meier, C. Schneider, S. Hofling, S. Schumacher, Realization of all-optical vortex switching in exciton-polariton condensates. *Nature Communications* **11,** 897 (2020).

[44] Y. del Valle-Inclan Redondo, C. Schneider, S. Klembt, S. Höfling, S. Tarucha, M. D. Fraser, Optically driven rotation of exciton-polariton condensates. *Nano Letters* **23,** 4564-4571 (2023).

[45] N. H. M. Dang, S. Zanotti, E. Drouard, C. Chevalier, G. Trippé-Allard, M. Amara, E. Deleporte, V. Ardizzone, D. Sanvitto, L. C. Andreani, C. Seassal, D. Gerace, H. S. Nguyen, Realization of polaritonic topological charge at room temperature using polariton bound states in the continuum from perovskite metasurface. *Advanced Optical Materials* **10,** 2270021 (2022).

[46] F. Manni, K. G. Lagoudakis, T. K. Paraïso, R. Cerna, Y. Léger, T. C. H. Liew, I. A. Shelykh, A. V. Kavokin, F. Morier-Genoud, and B. Deveaud-Plédran, Spin-to-

orbital angular momentum conversion in semiconductor microcavities, *Physical Review B* **83,** 241307(R) (2011).
[47] J. Wang, H. Xu, R. Su, Y. Peng, J. Wu, T. C. H. Liew, Q. Xiong, Spontaneously coherent orbital coupling of counterrotating exciton polaritons in annular perovskite microcavities. *Light: Science & Applications* **10,** 45 (2021).
[48] Terç H. Terças, H. Flayac, D. D. Solnyshkov, G. Malpuech, Non-Abelian gauge fields in photonic cavities and photonic superfluids. *Physical Review Letters* **112,** 066402 (2014).
[49] K. Alexey, M. Guillaume, and G. Mikhail, Optical spin Hall effect. *Physical Review Letters* **95,** 136601 (2005).
[50] C. Leyder, M. Romanelli, J. Ph. Karr, E. Giacobino, T. C. H. Liew, M. M. Glazov, A. V. Kavokin, G. Malpuech, and A. Bramati, Observation of the optical spin Hall effect. *Nature Physics* **3,** 628-631 (2007).
[51] E. Kammann, T. C. H. Liew, H. Ohadi, P. Cilibrizzi, P. Tsotsis, Z. Hatzopoulos, P. G. Savvidis, A. V. Kavokin, and P. G. Lagoudakis, Nonlinear optical spin Hall effect and long-range spin transport in polariton lasers. *Physical Review Letters* **109,** 036404 (2012).
[52] X. Ma, Y. V. Kartasho, A. Kavokin, S. Schumacher, Chiral condensates in a polariton hexagonal ring. *Optics Letters* **45,** 5700-5703 (2020).
[53] S. Dufferwiel, F. Li, E. Cancellieri, L. Giriunas, A. A. P. Trichet, D. M. Whittaker, P. M. Walker, F. Fras, E. Clarke, J. M. Smith, M. S. Skolnick, D. N. Krizhanovskii, Spin Textures of Exciton-polaritons in a tunable microcavity with large TE-TM splitting. *Physical Review Letters* **115,** 246401 (2015).
[54] M. Król, I. Septembre, P. Oliwa, M. Kędziora, K. Łempicka-Mirek, M. Muszyński, R. Mazur, P. Morawiak, W. Piecek, P. Kula, W. Bardyszewski, P. G. Lagoudakis, D. D. Solnyshkov, G. Malpuech, B. Piętka, J. Szczytko, Annihilation of exceptional points from different Dirac valleys in a 2D photonic system. *Nature Communications* **13,** 5340 (2022).
[55] S. Yao, Z. Wang, Edge states and topological invariants of non-Hermitian systems. *Physical Review Letters* **121,** 086803 (2018).
[56] P. Kokhanchik, D. Solnyshkov, G. Malpuech, Non-Hermitian skin effect induced by Rashba-Dresselhaus spin-orbit coupling. *Physical Review B* **108,** L041403 (2023).
[57] R. Bao, H. Xu, W. Verstraelen, T. C. H. Liew, Topological enhancement of exciton-polariton coherence with non-Hermitian morphing, *Physical Review B* **108,** 235305 (2023).
[58] M. Galbiati, L. Ferrier, D. D. Solnyshkov, D. Tanese, E. Wertz, A. Amo, M. Abbarchi, P. Senellart, I. Sagnes, A. Lemaitre, E. Galopin, G. Malpuech, J. Bloch, Polariton condensation in photonic molecules. *Physical Review Letters* **108**, 126403 (2012).
[59] L. Ferrier, E. Wertz, R. Johne, D. D. Solnyshkov, P. Senellart, I. Sagnes, A. Lemaître, G. Malpuech, J. Bloch, Interactions in confined polariton condensates. *Physical Review Letters* **106,** 126401 (2011).
[60] V. G. Sala, D. D. Solnyshkov, I. Carusotto, T. Jacqmin, A. Lemaître, H. Terças, A. Nalitov, M. Abbarchi, E. Galopin, I. Sagnes, J. Bloch, G. Malpuech, and A. Amo, Spin-orbit coupling for photons and polaritons in microstructures. *Physical Review X* **5**, 011034 (2015).
[61] Ge, L.; Nersisyan, A.; Oztop, B.; Tureci, H. E. Pattern formation and strong nonlinear interactions in exciton-polariton condensates. arXiv. 2013-11-19. https://arxiv.org/abs/1311.4847 (accessed 2026-01-05)
[62] A. V. Nalitov, H. Sigurdsson, S. Morina, Y. S. Krivosenko, I. V. Iorsh, Y. G. Rubo, A. V. Kavokin, I. A. Shelykh, Optically trapped polariton condensates as semiclassical time crystals. *Physical Review A* **99**, 033830 (2019).
[63] L. Polimeno, G. Lerario, M. De Giorgi, L. De Marco, L. Dominici, F. Todisco, A. Coriolano, V. Ardizzone, M. Pugliese, C. T. Prontera, V. Maiorano, A. Moliterni, C. Giannini, V. Olieric, G. Gigli, D. Ballarini, Q. Xiong, A. Fieramosca, D. D. Solnyshkov, G. Malpuech, D. Sanvitto, Tuning of the Berry curvature in 2D perovskite polaritons. *Nature Nanotechnology* **16,** 1349 (2021).
[64] M. Król, H. Sigurdsson, K. Rechcińska, P. Oliwa, K. Tyszka, W. Bardyszewski, A. Opala, M. Matuszewski, P. Morawiak, R. Mazur, W. Piecek, P. Kula, P. G. Lagoudakis, B. Piętka, J. Szczytko, Observation of second-order meron polarization textures in optical microcavities. *Optica* **8,** 255-261 (2021).
[65] K. Łempicka-Mirek, M. Król, H. Sigurdsson, A. Wincukiewicz, P. Morawiak, R. Mazur, M. Muszyński, W. Piecek, P. Kula, T. Stefaniuk, M. Kamińska, L. De Marco, P. G. Lagoudakis, D. Ballarini, D. Sanvitto, J. Szczytko, B. Piętka, Electrically tunable Berry curvature and strong light-matter coupling in liquid crystal microcavities with 2D perovskite. *Science Advances* **8,** eabq7533 (2022).
[66] N. Carlon Zambon, P. St-Jean, M. Milićević, A. Lemaître, A. Harouri, L. Le Gratiet, O. Bleu, D.D. Solnyshkov, G. Malpuech, I. Sagnes, S. Ravets, A. Amo, J. Bloch, Optically controlling the emission chirality of microlasers. *Nature Photonics* **13,** 283-288 (2019).
[67] Casalengua, E. Z.; Laussy, F. P. Spatial correlations of vortex quantum states. arXiv. 2024-02-02. https://doi.org/10.48550/arXiv.2402.01627 (accessed 2026-01-05).

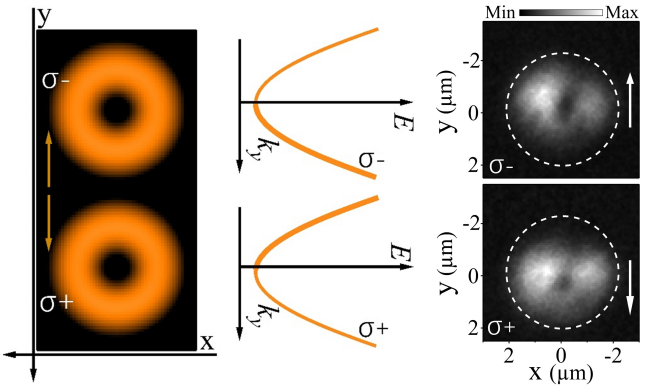

. **TOC Graphic**